ELSEVIER

Contents lists available at ScienceDirect

Separation and Purification Technology

journal homepage: www.elsevier.com/locate/seppur



Nanoparticle filtration through microporous ECTFE membrane in an alcoholic solution



Na Yao^a, Boris Khusid^{a,*}, Kamalesh K. Sirkar^{a,*}, Derek J. Dehn^b

- A Otto York Department of Chemical, Biological and Pharmaceutical Engineering, New Jersey Institute of Technology, University Heights, Newark, NJ 07102, USA
- b 3M Corporate Research Process Laboratory, 3M Center Building 219-1S-01, St. Paul, MN 55144, USA

ARTICLE INFO

Keywords: ECTFE membrane Solvent resistant membrane Cross-flow microfiltration of silica nanoparticles Alcoholic solution Fouling mechanisms

ABSTRACT

Organic solvent filtration is an important industrial process. It is widely used in pharmaceutical manufacturing, chemical processing industry, semiconductor industry, auto assembly etc. Most of the particle filtration studies reported in open literature dealt with aqueous suspension medium. The current work has initiated a study of cross-flow solvent filtration behavior of microporous ethylene chlorotrifluoroethylene (ECTFE) membranes using 12 nm silica nanoparticles suspended in an aqueous solution containing 25% ethanol. In the constant pressure mode of operation of cross-flow microfiltration (MF), permeate samples were collected at different time intervals. The permeate particle size distribution (PSD) results for different experiments were identical. Particle agglomerates having less than 100 nm size can pass through the membrane; some fouling was observed. The governing fouling mechanisms for tests operated using $3.8 \times 10^{-3} \, \text{kg/m}^3$ (3.8 ppm) at $6.9 \times 10^3 \, \text{Pag}$ and 1.4×10^4 Pag were pore blocking. For tests conducted using 3.8×10^{-3} kg/m 3 (3.8 ppm) at 27.6×10^3 Pag (4 psig) and 1.9×10^{-3} kg/m³ (1.9 ppm) at 6.9×10^{3} , 13.8×10^{3} and 27.6×10^{3} Pag (1, 2 and 4 psig), the mechanism was membrane resistance control. Less particles got embedded in membrane pores in experiments operated using suspensions with lower or higher particle concentrations with a higher transmembrane pressure. This is in good agreement with the values of the shear rate in the pore flow and scanning electron microscope images of the membrane after MF. In the dead-end mode of operation of solvent filtration using methanol, ethanol and 2-propanol, the permeate flux behavior follows $J_{methanol} > J_{ethanol} > J_{2-propanol}$ at all testing pressures. The values of permeance (kg/m²-s-Pa) determined from the slope of the linear plot of filtration flux vs. the applied pressure difference across the membrane, were 3.9×10^{-4} , 2.3×10^{-4} and 3.0×10^{-5} for methanol, ethanol and 2-propanol, respectively. Further exploration was made on solvent sorption results reported earlier. The critical temperature of selected solvents shows a better correlation with solvent sorption rather than the solubility parameter.

1. Introduction

Membrane is a selective separation barrier, which allows some component(s) to pass through but ideally prevents the rest [1] when some driving force is applied. The driving force is usually a difference in hydraulic pressure, partial pressure, composition or an electrical potential gradient or temperature gradient across the membrane. Applications of membranes for liquid separations have been widely developed resulting in a variety of membranes for reverse osmosis (RO), nanofiltration (NF), ultrafiltration (UF), microfiltration (MF), etc. based on the nominal pore size of the membrane. The pore size of MF membranes is about 0.02–10 μm . A relatively low feed operating pressure of approximately 1.03–4.14 \times 10 5 Pa (15–60 psig) can be applied to the feed for separation by a MF membrane. An extensive earlier review of

various aspects of MF are available in Chapters 31–35 of Ho and Sirkar [2].

For dead-end microfiltration of microbial suspensions, Foley [3] has done a review of various factors, including cell size and shape, cell surface properties, ionic environment, fermentation medium components and aging effects, affecting filter cake properties. In cross-flow microfiltration study by Field et al. [4], the concept of critical flux was introduced. It is the flux below which membrane fouling does not occur; however, above it a decline of flux is observed with time [4]. Theory, experiments and applications of critical and sustainable fluxes have been reviewed by Bacchin et al. [5]. Microfiltration of suspensions of paper mill effluent, biologically treated waste water, activated sludge, lactic acid fermentation broths, skimmed milk, natural organic matter, bovine serum albumin, myoglobin, silica, yeast, clay, latex, organic

E-mail addresses: khusid@njit.edu (B. Khusid), sirkar@njit.edu (K.K. Sirkar).

^{*} Corresponding authors.

matter, etc. have been reviewed [5]. However, the medium of most suspensions in the studies reported in open literature is water.

The stability of suspension is a precondition to a successful MF test. Variations of pH and ionic strength are widely used to maintain the stability of the suspension based on the net energy of interaction between surfaces. In research conducted by Elzo et al. [6], high permeate flux was obtained at high pH and low salt concentration, where the repulsion between the silica particles was strong. Moreover, the dissociation of the silanol groups Si-OH generated negatively charged Si-O $^-$ groups, which would change the net charge in the suspension with the addition of cations such as Ca^{2+} [6].

One of the principal applications of microporous membranes is MF: it is widely used for purification of processing fluids and removal of particles from acids, bases and organic solvents. There are a large number of articles published in this area [7-10]. Unfortunately, publications of MF in an organic environment is quite limited compared to those involving aqueous suspensions. Dutczak et al. [11] have successfully developed a technique that combines membrane formation and crosslinking reaction of fabricating fibers, which are more hydrophilic and attractive in alcohol system. Filtration performances of ECTFE membrane have been successfully studied by Ursino et al. [12] using pure solvents such as, methanol, ethanol and dimethylformamide due to the low degree of swelling of dense membranes in these solvents. This study did not involve any particle filtration. Among many other aspects studied, Karkhanechi et al. [13] made a very brief study of filtration of monosized latex-containing stabilized aqueous suspensions through hollow fibers fabricated from HALAR® ECTFE 901. Before studying the performance for particle removal by a membrane, solvent resistance and filtration in that media should be known. Our previous studies of ECTFE membrane suggested that it has excellent solvent resistance based on the study of solvent sorption properties, wetting characteristics, thermal resistance, electrical properties and mechanical properties [14]. Therefore, it is useful to explore filtration performances of ECTFE MF membranes in different media such as organic solvents. After that, nanoparticle filtration needs to be studied in both aqueous, aqueous-organic and non-aqueous media.

The relatively new microporous (MF) membrane of interest here is made of ECTFE (ethylene chlorotrifluoroethylene). The relative usefulness of ECTFE material-based MF membrane vis-à-vis those of other fully fluorinated and partially fluorinated fluoropolymers has been discussed earlier [14]. It is useful to have a perspective of the effects of a variety of organic solvents, pH variations and gamma radiation on the properties of microporous ECTFE membranes; comparison with commonly used polyvinylidene fluoride (PVDF) based membranes may also be carried out for selected properties. Table 1 provides a comparison of various properties between ECTFE and other fluoropolymers, such as, PVDF, fluorinated ethylene propylene (FEP) and perfluoroalkoxy (PFA). ECTFE membranes seem to behave better in most cases. Several researchers have successfully prepared ECTFE membranes via thermally

Table 1 ECTFE and a few other fluoropolymers: Comparison of various properties.

Articles	Properties	Performance
Yao et al. [14]; Extrand [15]; Drioli et al. [16]; *Yao et al. [17]	Chemical resistance	ECTFE is better than PVDF *ECTFE shows good TOA (tri-n- octylamine) resistance in the presence of a diluent
Yao et al. [14]	Wetting property	ECTFE is more hydrophobic and shows stronger wetting resistance
Drioli et al. [16]	Water recovery	ECTFE shows similar performance compared with PVDF
Lee et al. [18]	Yield stress, tensile strength	ECTFE is better than FEP, PFA
Hedenqvist et al. [19]	HCl, HBr resistance	ECTFE: unaffected; PVDF: less ductile

induced phase separation (TIPS). A summary of various studies of ECTFE membrane preparation including those of hollow fibers and their applications are provided in Table 2.

In general, membrane thickness, porosity, nominal pore size, liquid entry pressure (LEP), bubble point pressure, maximum pore size etc. need to be characterized for a given membrane [26]. Table 3 summarizes such information reported earlier [14] for ECTFE membranes used here. This study focuses on the cross-flow microfiltration behavior of suspensions of 12 nm silica nanoparticles in an alcoholic solution containing 25% alcohol in water. Our earlier microfiltration study explored briefly dead-end filtration of nanoparticles in water through ECTFE membrane which had been subjected to considerable swelling by tri-n-octylamine among other solvents. It was focused much more on understanding the effects of solvent swelling on a variety of properties of ECTFE membrane. Here we focus on cross-flow microfiltration behavior of this ECTFE membrane for nanoparticle suspensions in an aqueous/organic solvent mixture of 25% alcohol in water.

2. Experimental

2.1. Materials and chemicals

Hydrophobic ECTFE membranes (3 M, St. Paul, MN) with a nominal pore size of 0.2 μm and a thickness of $\sim 5 \times 10^{-5}\, m$ were used in this study. Organic solvents methanol, ethanol and 2-propanol, acetone, ethyl acetate, isopropyl acetate, acetonitrile and tetrahydrofuran (THF), heptane, toluene, p-xylene and chlorobenzene from Sigma-Aldrich (St. Louis, MO) were used previously in solvent sorption study [14]. Hydrophilic silica nanoparticles with a primary particle size of 12 nm (Aerosil 200, Evonik, Parsippany, NJ), surfactant sodium dodecyl sulfate (SDS) and ethanol were used to prepare suspensions to study the MF behavior of ECTFE membrane.

2.2. Solvent uptake analysis

Static solvent sorption test is important and necessary for applications where membranes are exposed to solvents. Experimental procedures and results were reported earlier [14,27]. Here, the solvent uptake of ECTFE membrane was analyzed with critical temperature and solubility parameter for various solvents. Selected solvents are grouped into polar protic solvents (methanol, ethanol and 2-propanol), polar aprotic solvents (acetone, ethyl acetate, isopropyl acetate, acetonitrile and THF) and nonpolar solvents (heptane, toluene, p-xylene and chlorobenzene). The solvent uptake of ECTFE membrane was explored with Hansen solubility parameter and sorption coefficient (S_{im}) or solubility coefficient which illustrates the extent of solubility/sorption of a solvent species in a membrane. Eqs. (1)–(3) show the calculation method for solubility coefficient for porous ECTFE membrane for various solvents.

$$V_{s} = \frac{m_{s}}{\rho_{s}} \tag{1}$$

$$V_{\rm m} = V(1-\varepsilon) \tag{2}$$

$$S_{im} = \frac{V_s}{V_m P_{vap}} \tag{3}$$

Here V_s is the volume of solvent that is sorbed in the solid membrane phase, m_s is the weight gain due to solvent sorption, ρ_s is the density of solvent, V_m is the actual membrane volume, V_m is the volume of the sample based on sample dimensions, ε is the porosity of the membrane (0.65 [14] was used here) and P_{vap} is the vapor pressure of each solvent at the testing temperature.

Table 2Overview of ECTFE flat/hollow fiber membrane preparation and applications.

Articles	Preparation	Application/ Innovation
Pan et al. [20]	Diluent mixture of ECTFE with bis(2-ethylhexyl) adipate (DEHA)/diethyl phthalate (DEP) via TIPS	Excellent fouling-resistance was observed during vacuum membrane distillation.
Pan et al. [21]	Homogeneous solution of ECTFE, SiO ₂ particle, composite powder (mixture of nanosized KCl and SiO ₂ particles) and diocyl adipate (DOA) via TIPS	Ultrafiltration performance was improved with the addition of additives.
Simone et al. [22]	Mixture of ECTFE with N-methyl pyrrolidone (NMP) with four different plasticizer additives, glycerol triacetate (GTA), triethyl citrate (TEC), dibutyl itaconate (DBI) and diethyl adipate (DEA) via TIPS	Pervaporation of toluene/water mixture showed that the best selectivity toward toluene is 4628 at 40 mbar with the addition of triacetin.
Drioli et al. [16]	Mixture of ECTFE with GTA via TIPS	Used in a membrane condenser for recovery of water from humidified gas streams
Zhou et al. [23]	Mixture of ECTFE with dibutyl sebacate (DBS) and triphenyl phosphite (TPP) via TIPS	Filtration measurement with water
Karkhanechi et al. [13]	Mixture of ECTFE with DEP and GTA via TIPS	Water permeability and particle rejection
Falbo et al. [24]	Mixture of ECTFE with NMP via TIPS	Pervaporation of a binary azeotropic mixture of ethanol and cyclohexane.
Pan et al. [25] Ursino et al. [12]	Mixture of ECTFE with DEHA, DEP and ${ m SiO_2}$ particles via TIPS Mixture of ECTFE with DEA via TIPS	Oil/water separation Solvent filtration

Table 3Basic properties of ECTFE membrane studied.

ECTFE membrane	Thickness	Porosity	Nominal pore size	LEP*	Bubble point pressure**
Value	$\sim\!5\times10^{-5}\text{m}$	65%	0.2 μm	$393\times10^{-3}Pag$	$127\times 10^{-3}\text{Pag}$

^{*} Liquid entry pressure was measured using water.

2.3. Microfiltration study

Microfiltration tests were carried out in two modes: dead-end and cross-flow. Pure solvents methanol, ethanol and 2-propanol were studied in dead-end microfiltration. The experimental setup is the same used earlier for liquid entry pressure (LEP) measurement [14]. The permeability constant or permeance was determined from Eqs. (4) and (5) [28,29]:

$$J = \frac{m}{At}$$
 (4)

$$J = \frac{Q}{\delta} \Delta P \tag{5}$$

Here, J is the filtration flux; m is the mass of the permeate collected during a certain time, t; A is the effective membrane area of the filtration cell; Q is the permeability coefficient; δ is the membrane thickness; $\triangle P$ is the applied pressure difference across the membrane. The quantity (Q/δ) is the permeability constant or permeance; it can be determined from the slope of a linear plot of J against ΔP . It has to be noted that the unit of filtration flux here is expressed based on mass, kg/m²-s, instead of volume e.g., L/m²-h (LMH); this approach was used because weighing is easier and more accurate, especially in the crossflow mode of operation where the permeate samples are silica suspensions with different densities/concentrations. Therefore, it is more convenient to express the filtration flux using mass, instead of volume.

Particle filtration was studied in cross-flow microfiltration mode, which is schematically shown in Fig. 1. Silica nanoparticle suspension was used in the current study. The methods for suspension preparation and particle size distribution (PSD) measurement conducted using a Malvern Zetasizer (Nano series, Westborough, MA) were the same as those reported earlier [17] except 25% ethanol-75% water was used to make the suspension instead of pure water. Due to the hydrophobicity of ECTFE membrane, an organic solvent such as ethanol was added to the suspension to "wet" the membrane. From LEP results of ECTFE membrane [14], $3.93 \times 10^5 \, \mathrm{Pag}$ (57 psig) is the LEP value of pure water and $5.17 \times 10^4 \, \mathrm{Pag}$ (7.5 psig) is the value of 25% ethanol (75% water).

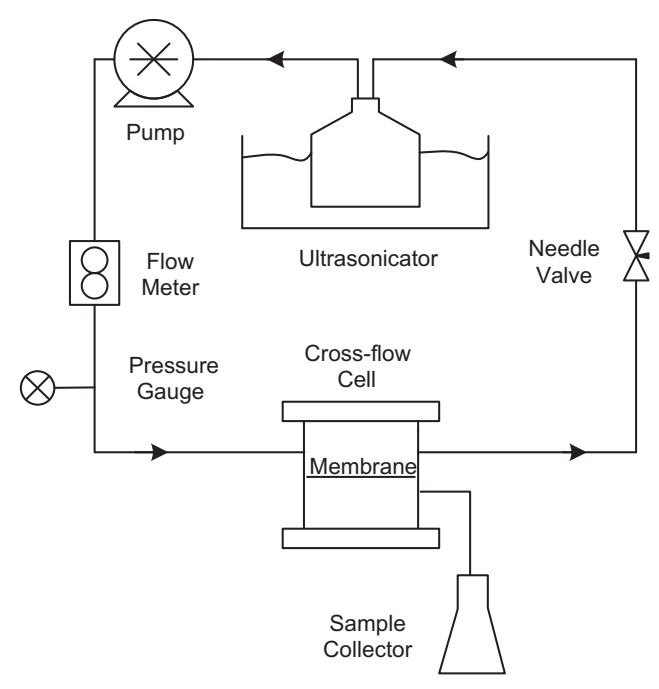


Fig. 1. Experimental set-up for cross-flow microfiltration.

One needs 35% of ethanol to get the membrane wetted [14].

According to Darcy's law, the permeation flux of a feed flowing along across a membrane can be described by

$$J = \frac{\Delta P}{\mu R_t} \tag{6}$$

Here, μ is the viscosity of the feed; R_t is the total hydraulic resistance over the entire membrane. For a microfiltration test using suspensions, R_t is usually the sum of the resistances caused by membrane itself (R_m) , pore blocking (R_p) and cake formation (R_c) [30]. Therefore, Eq. (6) can

^{**} Liquid entry pressure was measured using pure 2-propanol.

be written in the following form:

$$J = \frac{\Delta P}{\mu (R_{\rm m} + R_{\rm p} + R_{\rm c})} \tag{7}$$

Flux decline is a major problem in microfiltration. As shown in Eq. (7), the membrane itself, pore blocking and cake formation could cause flux reduction. According to Wiesner et al. [31] and Lim et al. [30], the behavior of the permeation flux based on different fouling mechanisms can be summarized as:

Membrane resistance-limited:
$$\frac{1}{J} = \frac{1}{J_0} + K_m t$$
 (8)

Pore blocking resistance-limited:
$$I = -K_p t + \ln J_0$$
 (9)

Cake resistance-limited:
$$\frac{1}{J^2} = \frac{1}{J_0^2} + K_c t$$
 (10)

Here, J_0 is the initial flux; K_m , K_p and K_c are the parameters that are respectively related to the resistances of the membrane itself, pore blocking and cake formation.

Eqs. (11) and (12) [32,33] used to calculate the wall shear stress (τ_w) and wall shear rate (γ) through a cylindrical pore are expressed as:

$$\tau_{\rm w} = \frac{\rm R\Delta P}{\rm 2L} \tag{11}$$

$$\gamma = \frac{R\Delta P}{2\mu L} \tag{12}$$

Here, R is the radius of membrane pore assumed to be straight and cylindrical; $\triangle P$ is the applied pressure difference over the membrane; L is the membrane thickness; μ is the viscosity of the feed suspension. Since the suspension is very dilute, the viscosity of the solvent can be used here. However, the viscosity of dilute suspension can be determined from Einstein Eq. [34]:

$$\frac{\mu}{\mu_0} = 1 + \frac{5}{2}\emptyset \tag{13}$$

Here, μ_o is the viscosity of the liquid medium of the suspension and \emptyset is the volume fraction of the solids in the suspension. It needs to be mentioned that Eq. (13) is valid only when particles are rigid spheres and the suspension is dilute, namely $\emptyset < 0.05$.

The effects of operating conditions such as suspension concentration and transmembrane pressure on filtration flux were studied. Scanning electron microscopy (SEM) images were also taken with LEO 1530 VP field emission scanning electron microscope (Carl Zeiss Inc., Peabody, MA) for the membranes after microfiltration was finished. All membrane samples were coated with carbon using a turbo-pumped sputter and carbon coater (EMS 150 T ES, Hatfield, PA) prior to image collection.

3. Results and discussion

3.1. Solvent uptake analysis

The extent of solvent uptake of ECTFE membranes by selected solvents was reported earlier [14] in terms of solvent sorption. Solvent sorption coefficient was calculated from those data by Eq. (3) and plotted. Fig. 2 shows the relationship between sorption coefficient and the critical temperature (T_c) based on the selected solvents. Generally, the higher the T_c , the higher is the solubility. In general, a larger solvent species with a higher boiling point would have a higher condensability. This is often correlated with a higher critical temperature (T_c). Therefore, it would result in a higher solubility [16]. Fig. 3(a and b) illustrates the relationship of membrane weight gain vs. solubility parameter for polar protic solvents and nonpolar solvents, respectively. Generally, Fig. 3(a) indicates that the higher the hydrophobicity of the solvent, the lower is the solubility parameter (δ) and the higher is the

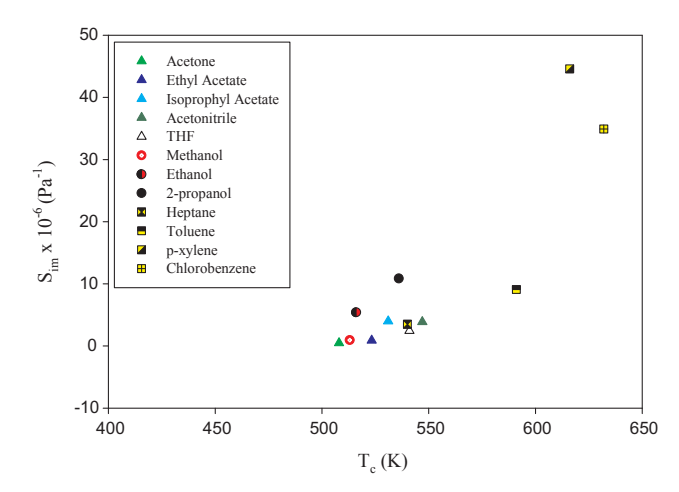


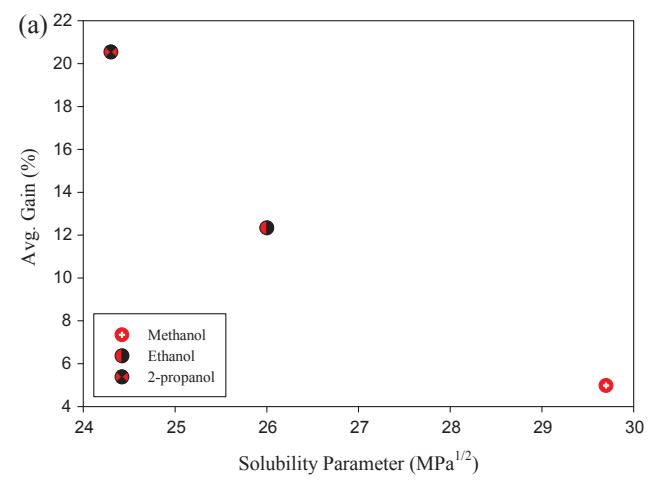
Fig. 2. Overview of the correlation between membrane sorption coefficient and critical temperature for various solvents and ECTFE membrane.

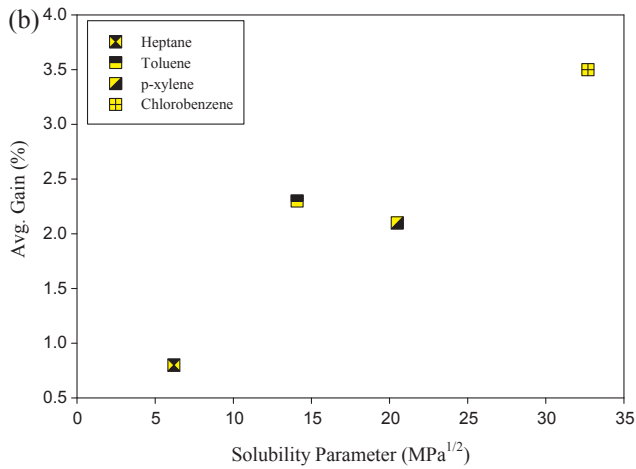
weight gain. On the other hand, Fig. 3(b) shows that alkanes and aromatic solvents having higher hydrophobicity and therefore lower solubility parameter have generally low weight gain. However, these two curves do not show a clear trend as is shown in Fig. 2. Fig. 3(c) illustrates the correlation between sorption coefficient vs. hydrogen bonding parameter (δ_h) for polar aprotic solvents. In general, the sorption coefficient increases with δ_h . Ursino et al. also reported similar results for acetone, n-methyl-2-pyrrolidone, dimethylacetamide and dimethylformamide [12].

Even though solubility parameter has been widely studied with solvent sorption behavior [35–39], all these studies involved swelling of rubbers. In the current study, for nonpolar solvents, generally, the extent of swelling of these solvents increase with Hansen solubility parameter [12,14]. Ebnesajjad reported that the extent of swelling of fluoropolymers, PTFE and FEP, by hydrogen-containing solvents is very limited (less than 1%); therefore, it does not depend on the solubility parameter [40]. Instead it depends on the chemical structure of the solvent; the higher the similarity of the solvent chemical structure and the fluoropolymer structure, the larger the swelling [40]. Additionally, the solubility parameter-based affinity of ECTFE membrane and the solvent has also been used to study the membrane-solvent interaction and solvent swelling/uptake [13]. Moreover, the interaction of ECTFE and the solvents is only physical because the removal of certain halogenated solvents from ECTFE can bring the mechanical properties back to its original state [40]. Such information will be useful when solventbased MF is implemented.

3.2. Solvent filtration in dead-end microfiltration mode

The solvents selected for these tests were methanol, ethanol and 2-propanol; their basic characteristics are summarized in Table 4. Based on a combination of Eqs. (4) and (5), the permeability constant (i.e., the permeance) can be determined. The results of solvent flux vs. pressure and the permeability constant are shown respectively in Fig. 4 and Table 4. In all tests, the permeate flux increased linearly with an increased pressure. The permeate flux comparison at all testing pressures follows $J_{\rm methanol} > J_{\rm ethanol} > J_{\rm 2-propanol}$, which is expected. Ursino et al. also reported similar solvent flux results for methanol and ethanol [12]. The permeability constant of these three solvents also behave in the same order as filtration flux. This behavior can be explained on the basis of different molecular weights and viscosities of the three solvents [12,42]. For example, the molecular weight and the viscosity of methanol are smaller than those of the other two solvents.





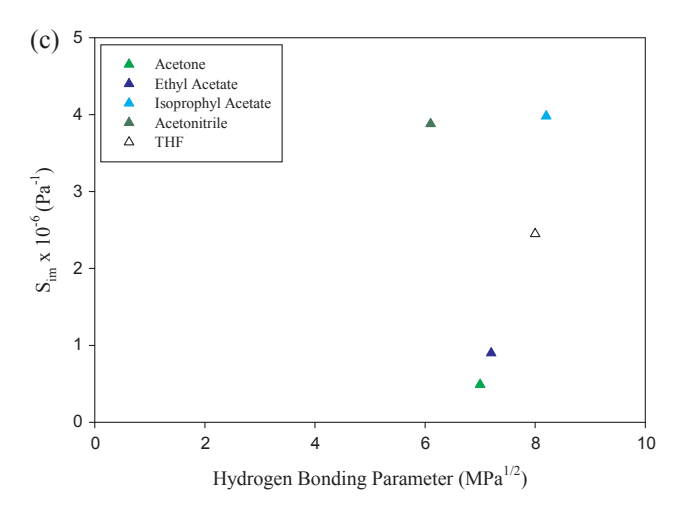


Fig. 3. Variation of membrane weight gain due to solvent sorption with respect to solubility parameter of (a) polar protic solvents and (b) nonpolar solvents and (c) correlation of sorption coefficient vs. hydrogen bonding parameter for polar aprotic solvents. Note: The values of solubility parameter were taken from Reference [41] and the hydrogen bonding parameter were taken from [38]; the values of Avg. Gain are reprinted from Reference [14].

3.3. Nanoparticle filtration in cross-flow microfiltration

Three runs with filtrate samples collected every 120 s (I), 180 s (II) and 300 s (III) have been carried out using a suspension of $3.8 \times 10^{-3}\,\text{kg/m}^3$ (3.8 ppm) silica in 25% ethanol solution at $1.03 \times 10^5\,\text{Pag}$ (15 psig). A comparison of the filtration fluxes illustrated in Fig. 5 shows that the runs

Table 4
Characteristics of the solvents used in filtration flux measurements.

Solvent	Molecular weight (g/ mol)	Density (kg/m³)	Surface tension* (mN/m)	Viscosity**(Pa-s)	Permeability constant (kg/ m²-s-Pa)
Methanol Ethanol 2-propanol	32.04 46.07 60.1	791 789 786	22.51 21.82 21.22	0.585×10^{-3} 1.201×10^{-3} 2.428×10^{-3}	3.9×10^{-4} 2.3×10^{-4} 3.0×10^{-5}

- * Adapted from Reference [43].
- ** Adapted from Reference [44].

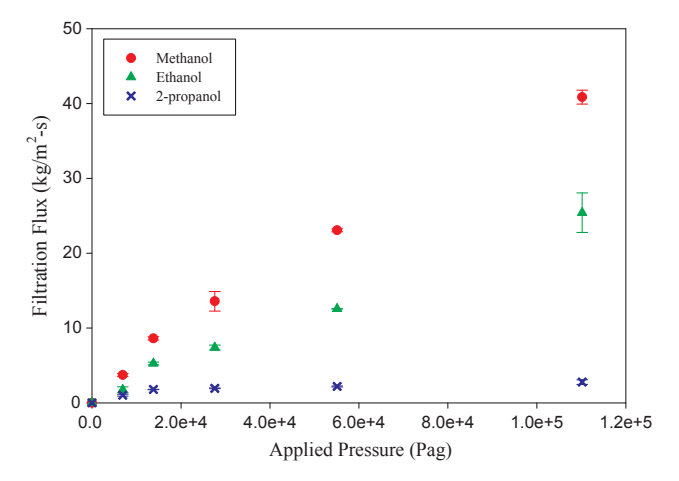


Fig. 4. Filtration flux of three alkanols at different pressures through ECTFE membrane.

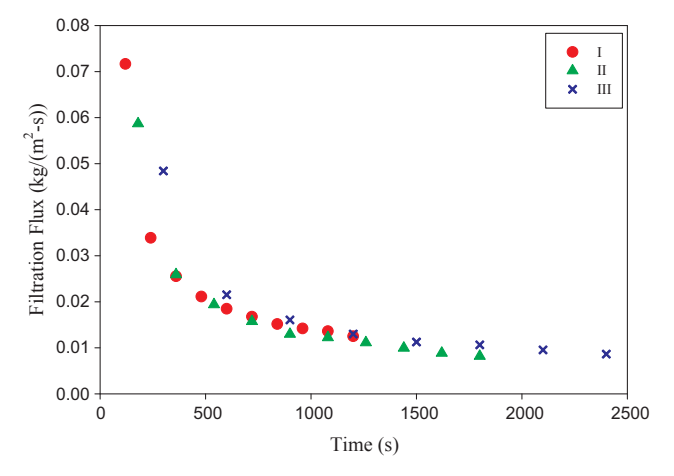


Fig. 5. Filtration flux comparison of cross-flow microfiltration at 1.03×10^5 Pag (15 psig) at three different sample collection intervals, 120 s (I), 180 s (II) and 300 s (III).

were reproducible in terms of filtration flux vs. time. Fig. 6(a-c) are the PSD overlay of feed and the filtrates collected every $120 \, s$, $180 \, s$ and $300 \, s$, respectively. The PSD of the feed indicates aggregation of the silica nanoparticles since the particle size distribution lies approximately in the range of $40-200 \, nm$. This corresponds to the basic size of the nanoparticle (NP) which is present as a fused agglomerate of $4 \, NPs$ due to fusion during their production process; larger aggregates are increasingly rejected. Therefore, sonication was applied to the feed reservoir during the measurements.

Fig. 7(a and b) provides a comparison of three different runs at around $600 \, s$ and $1200 \, s$, respectively. It appears that the three runs were quite similar especially at the time point of $1200 \, s$ (Fig. 7(b)). In addition, it seems that the particles with size larger than $200 \, nm$ cannot

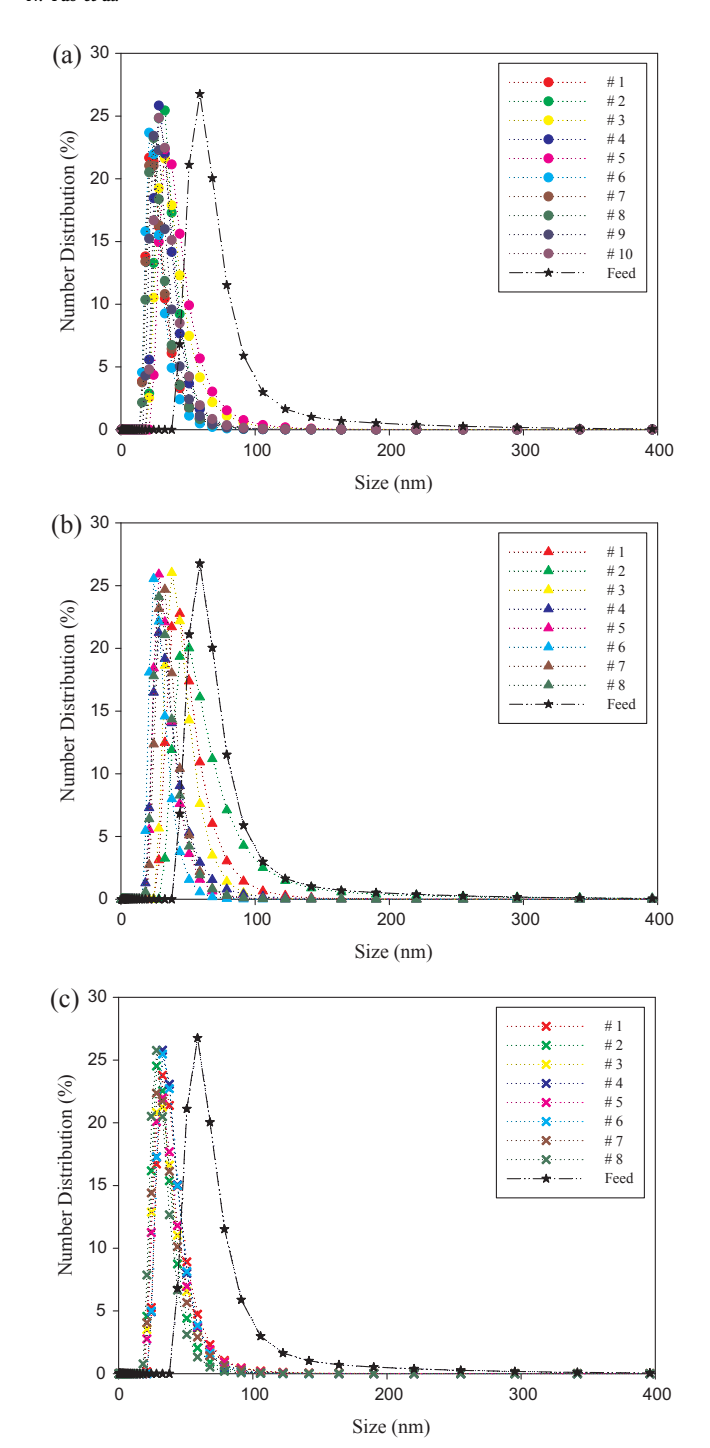
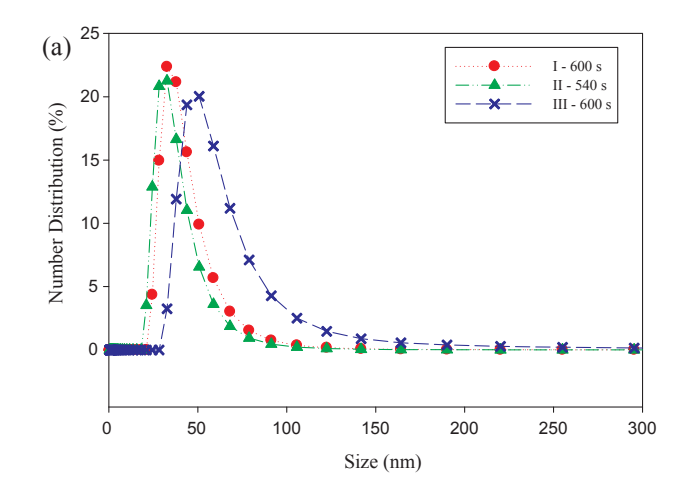


Fig. 6. The PSD results of filtrates collected every (a) $120 \, \text{s}$, (b) $180 \, \text{s}$ and (c) $300 \, \text{s}$

go through the membrane as far as Fig. 6(a–c) are concerned. This suggests that the nominal membrane pore size is 0.2 μm , as was determined from earlier studies [14]. It appears also that as time progressed, the PSD in the filtrate is being skewed slowly towards lower size with a peak at around 40–50 nm. Particles dispersed in aqueous ethanol solution were able to pass through the membranes at 1.03×10^5 Pag even after 2400 s in the cross-flow MF; however, no particles (in the media of water) could pass through ethanol-soaked ECTFE membrane in dead-end MF at the pressure of 3.5×10^5 Pag after 300 s [17]. This suggested that the fouling phenomenon in the cross-flow MF with the built-up cake was developed slowly and the membrane pores were blocked or partially blocked slowly compared with



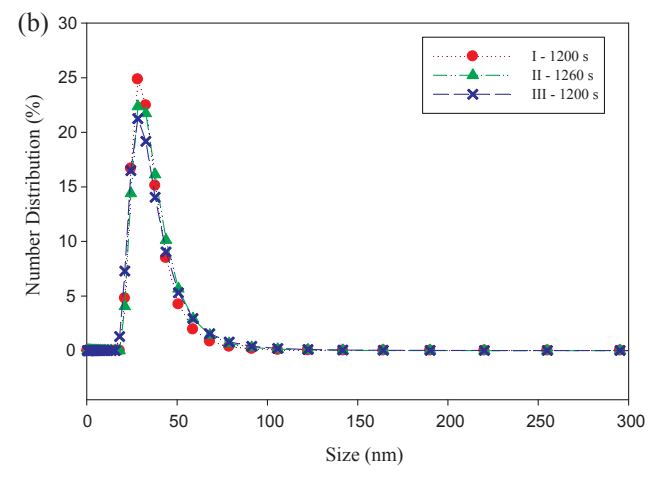


Fig. 7. The PSD comparison of three runs at around (a) 600 s and (b) 1200 s.

those in dead-end MF.

The effects of feed particle concentration in the suspension and the operating pressure were also studied. The feed flow rate was $5.0\times10^{-7}\,\text{m}^3/\text{s}$ for all tests. Fig. 8 illustrates the relationship between filtration flux and time for operation at different pressures using $3.8\times10^{-3}\,\text{kg/m}^3$ (3.8 ppm) and $1.9\times10^{-3}\,\text{kg/m}^3$ (1.9 ppm) silicaethanol suspensions. In Fig. 8, the flux obtained for operation under $6.9\times10^3\,\text{Pag}$ (1 psig) using $3.8\times10^{-3}\,\text{kg/m}^3$ (3.8 ppm) suspension had as expected the lowest flux value. Generally, the flux for all six runs shows the highest values and the highest decline rate at the beginning, and then the flux drops down gradually toward a plateau at the end. At the last 1200 s, the flux values stack up as follows: $J_{1.9\times10^{-3}\text{kg/m}^3-6.9\times10^{3}\text{pag}} > J_{3.8\times10^{-3}\text{kg/m}^3-2.8\times10^{4}\text{pag}} > J_{3.8\times10^{-3}\text{kg/m}^3-1.4\times10^{4}\text{pag}}$

 $>J_{3.8\times 10^{-3}kg/m^3-6.9\times 10^3Pag}$ as shown in the small inset figure in Fig. 8. Less fouling is observed in the case where filtration is operated under 2.8 \times 10^4 Pag (4 psig) using $1.9\times 10^{-3}\,kg/m^3$ (1.9 ppm) suspension.

The filtration results of these six runs were also plotted using Eqs. (8)–(10) to find out the governing fouling mechanism. The regression equations are shown in Table 5. Here y refers to the ordinate corresponding to Eqs. (8), (9) and (10) for the mechanism under consideration and x to time (see Fig. 9). The governing fouling mechanism for the experiments which was operated using $3.8 \times 10^{-3} \, \text{kg/m}^3$ (3.8 ppm) at $6.9 \times 10^3 \, \text{Pag}$ (1 psig) and $1.4 \times 10^4 \, \text{Pag}$ (2 psig) appears to be pore blocking. These two runs have the lowest values of the filtration flux at the last 1200 s. The governing mechanism for the remaining four runs is membrane resistance. Less particles get embedded

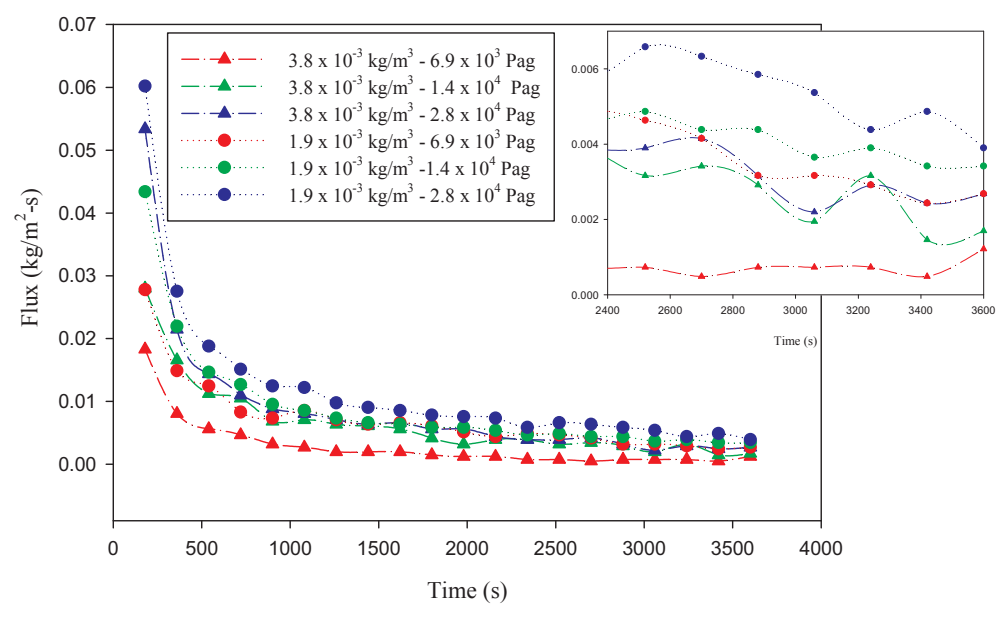


Fig. 8. The relationship between filtration flux and time operated at different pressures using different silica nanoparticle suspensions in aqueous ethanol.

in membrane pores in the experiments operated using suspensions with lower concentrations or somehow higher concentration with a higher transmembrane pressure. When the operating pressure is lower, the shear rate in the pore is lower. Therefore, more particles would get embedded in membrane pores. The cake formation mechanism is not the governing mechanism for any run. It reflects the intrinsic characteristics of cross-flow mode that the high wall shear rate on top of the membrane would lead to reduced deposition of particles on the membrane surface.

The plots of fouling mechanisms are shown in Fig. 9(a–d). At the beginning of the six runs, it appears that membrane itself has more impact on the permeate flux, as shown in Fig. 9(a) and (c). In this case, the clean membrane would be the major resistance. However, as time goes by, more and more particles get embedded in membrane pores. Thus, pore blocking mechanism plays a more important role, as shown in Fig. 9(b) and (d). This is consistent with the results reported by Lim et al. [30].

The values of inside-the-membrane-pore τ_w and γ calculated for different test conditions in this cross-flow microfiltration study are summarized in Table 6. As was mentioned earlier, the governing fouling mechanism of the tests operated using $3.8\times 10^{-3}\, kg/m^3$ (3.8 ppm) at $6.9\times 10^3\, Pag$ (1 psig) and $1.4\times 10^4\, Pag$ (2 psig) is pore blocking. Here it shows that these runs had relatively low value of $\gamma.$ In the tests operated using a more dilute suspension, the membrane itself plays a

more important role on fouling. For the tests $(3.8 \times 10^{-3} \, \text{kg/}$ ${\rm m}^{3}(3.8~{\rm ppm})$ – $2.8\times10^{4}~{\rm Pag}~(4~{\rm psig})~{\rm and}~1.9\times10^{-3}~{\rm kg/m}^{3}~(1.9~{\rm ppm})$ -2.8×10^4 Pag (4 psig)) with higher shear rates (25.2 \times 10³ and $27.1 \times 10^3 \, \mathrm{s^{-1}}$, respectively), less internal fouling is observed. It needs to be mentioned that the value of γ should be determined by using the exact applied pressure difference across the membrane. At the beginning of MF tests, there is no fouling. Thus, the values of applied pressure difference across the membrane 6.9×10^3 Pag, 1.4×10^4 Pag and 2.8×10^4 Pag (1, 2)and 4 psig) are the exact values of $\triangle P$ in Eq. (11). However, fouling was observed as time goes by. The internal pore blocking or the built-up cake would cause additional resistance over the entire membrane, and therefore, results in a decrease of velocity and shear rate through the pore for the same overall applied $\triangle P$; in effect the pressure drop over any one of the three resistances is changing with time. The results shown in Table 6 were calculated with the assumption that $\triangle P$ is constant during the MF process. Generally, the comparison of shear rates at different experimental times should be comparable to that at the beginning of MF. In this case, it can provide a broad guideline on the values of shear rate at different $\triangle Ps$. Generally, the higher the shear rate, the higher is the filtration flux. Therefore, the flux comparison for these six conditions should be $J_{1.9\times 10^{-3}kg/m^3-1.4\times 10^4Pag}>J_{3.8\times 10^{-3}kg/m^3-1.4\times 10^4Pag}>J_{1.9\times 10^{-3}g/m^3-6.9\times 10^3Pag}$ >J $_{3.8\times10^{-3}$ kg/m 3 - 6.9×10^{-3} Pag</sub>, however, it is not. The correct comparison has been concluded in Section 3.3. It turns out that the viscosity of the feed plays a more important role than the applied pressure difference across the

Table 5Regression results to test for membrane fouling mechanisms.

Test conditions	Mechanism				
	Membrane resistance-limited	Pore blocking resistance-limited	Cake resistance-limited		
$3.8 \times 10^{-3} \text{kg/m}^3$ - $6.9 \times 10^3 \text{Pag}$	y = 0.49x - 88.24	$y = -0.0008x - 4.82$ $R^2 = 0.8153$	$y = 886.59x - 606,064$ $R^2 = 0.5307$		
$3.8 \times 10^{-3} \text{kg/m}^3$ – $1.4 \times 10^4 \text{Pag}$	$R^2 = 0.7364$ y = 0.15x - 19.26 $R^2 = 0.8247$	$R^{-} = 0.8153$ $y = -0.0007x - 4.07$ $R^{2} = 0.8959$	$R^{2} = 0.5307$ y = 90.336x - 74,928 $R^{2} = 0.6051$		
$3.8 \times 10^{-3} \text{kg/m}^3 2.8 \times 10^4 \text{Pag}$	$R = 0.8247$ $y = 0.11x - 1.90$ $R^2 = 0.9211$	$x = 0.8939$ $y = -0.0007x - 3.82$ $R^2 = 0.8521$	$y = 48.801x - 34,771$ $R^2 = 0.7653$		
$1.9 \times 10^{-3} \text{kg/m}^3$ – $6.9 \times 10^3 \text{Pag}$	$x = 0.9211$ $y = 0.10x + 20.78$ $R^{2} = 0.936$	$y = -0.0021$ $y = -0.0005x - 4.12$ $R^2 = 0.8985$	$y = 41.113x - 26,893$ $R^2 = 0.8188$		
$1.9 \times 10^{-3} \text{kg/m}^3 - 1.4 \times 10^4 \text{Pag}$	$y = 0.07 \times + 28.89$ $R^2 = 0.9809$	$y = -0.0006x - 3.91$ $R^2 = 0.8277$	$y = 24.88x - 11,863$ $R^2 = 0.9479$		
$1.9 \times 10^{-3} \text{kg/m}^3 2.8 \times 10^4 \text{Pag}$	$y = 0.06x + 19.01$ $R^2 = 0.9602$	$y = -0.0006x - 3.63$ $R^2 = 0.8294$	$y = 15.347x - 8385.8$ $R^2 = 0.8645$		

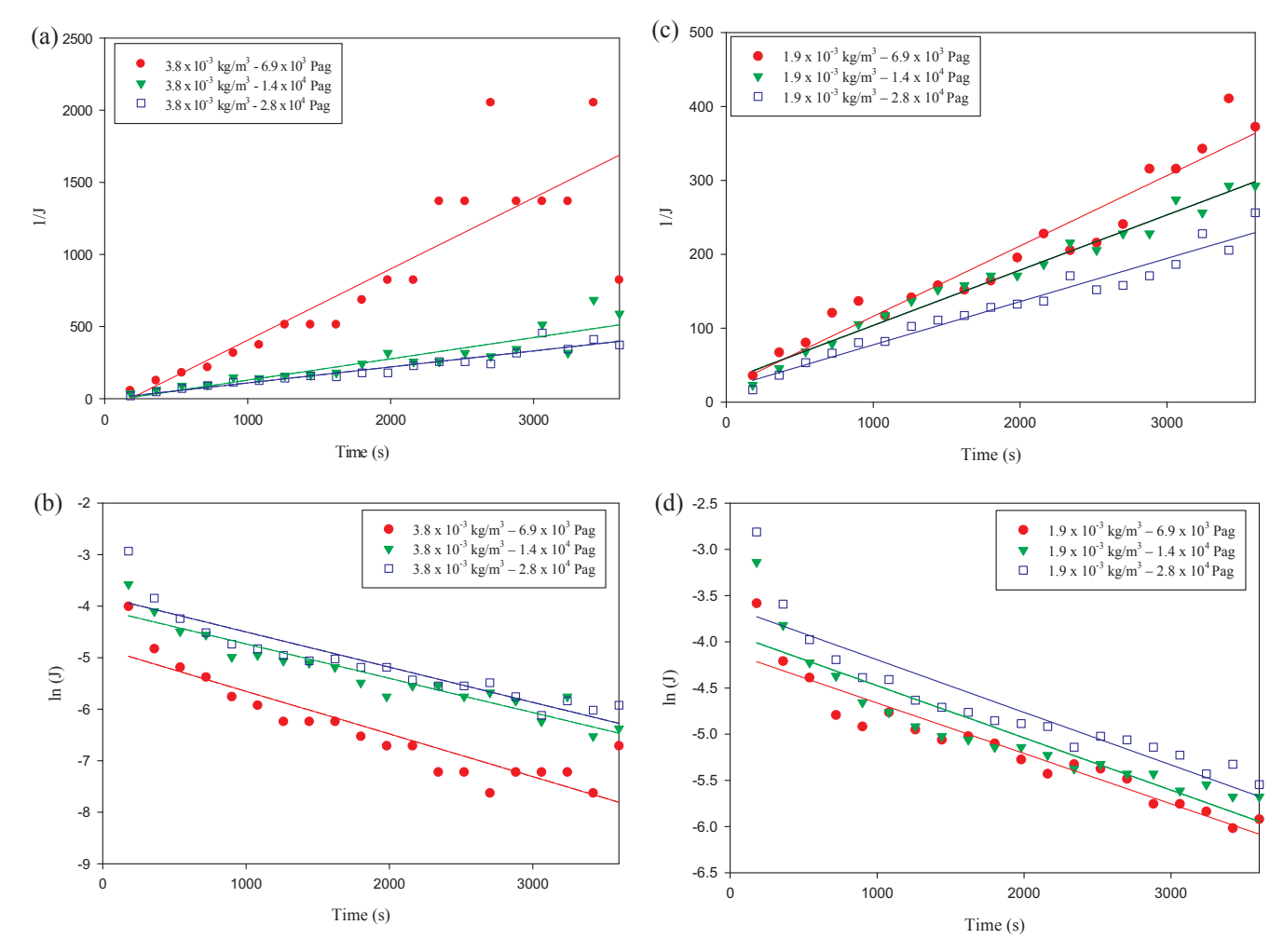


Fig. 9. Plots of fouling mechanisms: (a) membrane-limited model for $3.8 \times 10^{-3} \, \text{kg/m}^3$ (3.8 ppm) suspension, (b) pore-blocking model for $3.8 \times 10^{-3} \, \text{kg/m}^3$ (3.8 ppm) suspension, (c) membrane-limited model for $1.9 \times 10^{-3} \, \text{kg/m}^3$ (1.9 ppm) suspension and (d) pore-blocking model for $1.9 \times 10^{-3} \, \text{kg/m}^3$ (1.9 ppm) suspension.

Table 6 Values of τ_w and γ for different test conditions in cross-flow microfiltration.

Test conditions	τ _w (Pa)	γ (s ⁻¹)
$3.8 \times 10^{-3} \text{kg/m}^3 - 6.9 \times 10^3 \text{Pag}$	6.9	6.3×10^{3}
$3.8 \times 10^{-3} \text{kg/m}^3 - 1.4 \times 10^4 \text{Pag}$	13.8	12.6×10^{3}
$3.8 \times 10^{-3} \text{kg/m}^3 - 2.8 \times 10^4 \text{Pag}$	27.6	25.2×10^{3}
$1.9 \times 10^{-3} \text{kg/m}^3 - 6.9 \times 10^3 \text{Pag}$	6.9	6.8×10^{3}
$1.9 \times 10^{-3} \text{kg/m}^3 - 1.4 \times 10^4 \text{Pag}$	13.8	13.6×10^{3}
$1.9 \times 10^{-3} \text{kg/m}^3 2.8 \times 10^4 \text{Pag}$	27.6	27.1×10^{3}

membrane in the current study.

One may wonder about the maximum size of a particle that can pass through the membrane pores easily. When the nanoparticle diameter (48 nm) is not smaller than the membrane pore size (200 nm) by orders of magnitude, the effective diffusion coefficient is decreased by a drag factor G_{Dr} (r_p , r_m) [29]:

$$G_{Dr} = 1.1004 \left(\frac{r_p}{r_m}\right) + 2.089 \left(\frac{r_p}{r_m}\right)^3 - 0.948 \left(\frac{r_p}{r_m}\right)^5 + \cdots$$
 (14)

Here, r_p and r_m are the radius of nanoparticles and membrane pores, respectively. Based on the above equation, the particles with smaller size are likely to pass through the membrane pores. Note: this equation (Faxen Equation) is valid only when $(r_p/r_m) < 0.5$ among other assumptions.

Fig. 10 illustrates SEM images of ECTFE membrane before

microfiltration and after microfiltration tests using $3.8\times10^{-3}\,kg/m^3$ (3.8 ppm) silica-ethanol-water suspension at different pressures. Fig. 10(a and b) shows the SEMs of virgin membrane. Fig. 10(c–h) representing membranes subjected to MF clearly show that particles were deposited on the membrane surface or embedded in membrane pores compared with the pristine membranes (Fig. 10(a and b)). Obviously, the particle size in the permeates was smaller than that of the feed as shown in Fig. 6. Moreover, less number of particles were observed in Fig. 10(c and d). In this case, the membrane is cleaner than those of the other two. This is in good agreement with earlier results that the governing fouling mechanism for the experiment using $3.8\times10^{-3}\,kg/m^3$ (3.8 ppm) at $2.8\times10^4\,Pag$ (4 psig) is membrane resistance while for tests that operated at $6.9\times10^3\,Pag$ (1 psig) and $1.4\times10^4\,Pag$ (2 psig) the governing mechanism is pore blocking. Therefore, it is clear that the higher the operating pressure, the lower is the fouling of the membrane sample.

4. Concluding remarks

Organic solvent filtration is widely used in pharmaceutical manufacturing, chemical processing industry, semiconductor industry, auto assembly etc. Study of solvent resistance of membranes is necessary and useful. The aim of this research was to study the effect of processing parameters, such as feed concentration, applied pressure difference on cross-flow MF. Pure solvent filtration flux and flux with nanoparticles suspended in the alcoholic system are of great interest. Understanding of the solvent effect on ECTFE membrane is also important. The

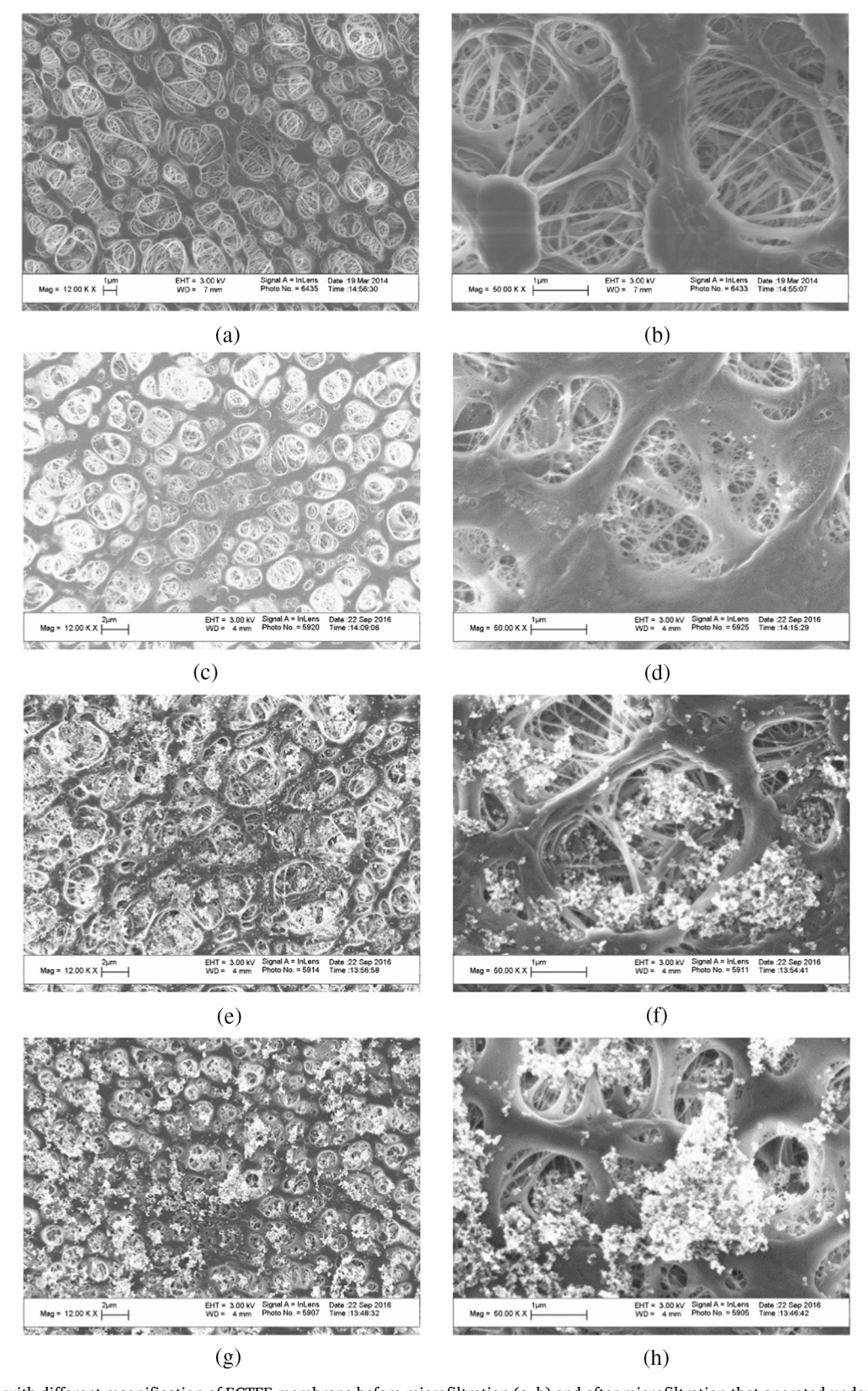


Fig. 10. SEM images with different magnification of ECTFE membrane before microfiltration (a, b) and after microfiltration that operated under (c, d) 2.8×10^4 Pag, (e, f) 1.4×10^4 Pag and (g, h) 6.9×10^3 Pag using 3.8×10^{-3} kg/m³ silica–aqueous ethanol suspension.

membrane sorption coefficients of various solvents for ECTFE membrane show a good correlation with the $T_{\rm c}$ of these solvents. In general, the higher the $T_{\rm c}$, the higher is the sorption/solubility. The weight gain of swollen ECTFE membranes did not show a good correlation with

solubility parameter of various solvents. Solvent uptake of glassy fluoropolymers by hydrogen-containing solvents is very limited. Generally, the higher the similarity of the solvent chemical structure with the fluoropolymer structure, the higher is the solvent uptake. This

provides general guidance about the affinity between the membrane and the solvent.

It is useful to know the basic properties of the membrane prior to solvent filtration. Dead-end filtration mode is a quick way to know the general behavior of a membrane as a filter. In dead-end microfiltration of ECTFE membranes operated using pure methanol, ethanol and 2propanol, the permeate solvent flux varies as $J_{methanol}\,>\,J_{ethanol}\,>\,J_{2\text{-}}$ propanol at all testing pressures. This can be explained by the different physical properties such as solvent molecular weights and their viscosities. The permeance or permeability constant was determined from the slope of the linear plot of filtration flux against the applied pressure difference across the membrane. The results for methanol, ethanol and 3.9×10^{-4} . 2-propanol are respectively 2.3×10^{-4} $3.0 \times 10^{-5} \,\text{kg/m}^2$ -s-Pa.

In constant pressure mode of operation of cross-flow microfiltration, permeate samples were collected at different time intervals. The PSD results at the same time were identical, which indicates reproducibility of this test. The particle agglomerates within the size of 100 nm can pass through the membrane; there is clear indication of some fouling, which is a slow process compared with dead-end MF. The governing fouling mechanisms for the tests operated using $3.8 \times 10^{-3} \, \text{kg/m}^3$ at 6.9×10^3 Pag (1 psig) and 1.4×10^4 Pag (2 psig) were pore blocking, while that for the tests conducted using $3.8 \times 10^{-3} \, \text{kg/m}^3$ (3.8 ppm) at $2.8 \times 10^4 \, \text{Pag}$ (4 psig) and $1.9 \times 10^{-3} \, \text{kg/m}^3$ (1.9 ppm) 6.9×10^3 Pag, 1.4×10^4 Pag and 2.8×10^4 Pag (1, 2 and 4 psig) were membrane resistance. Less particles get embedded in membrane pores in experiments operated using suspensions with lower concentrations or higher concentration with a higher transmembrane pressure. Regarding the values of shear rate, the two tests operated using $3.8 \times 10^{-3} \, \text{kg/m}^3$ (3.8 ppm) at 6.9×10^{3} Pag (1 psig) and 1.4×10^{4} Pag (2 psig) show relatively lower value. The fouling shown in the SEM images of the membrane after MF is in good agreement with earlier results. Particle filtration has been successfully carried out in cross-flow MF. ECTFE membrane is expected to be used more often in industries.

Acknowledgements

The authors gratefully acknowledge support for this research from the NSF Industry/University Cooperative Research Center for Membrane Science, Engineering and Technology that has been supported via NSF Award IIP1034710. We are grateful to Prof. Wen Zhang (NJIT) for sharing the instrument for particles size distribution measurement. Special thanks are due to Prof. Costas G. Gogos (NJIT) for constructive feedbacks. Na Yao was supported by NJIT during Fall 2016 - Fall 2017.

References

- [1] K.W. Böddeker, Liquid Separations with Membranes: An Introduction to Barrier Interference, Springer, 2008. W. Ho, K. Sirkar, Membrane Handbook, Chapman & Hall, New York, NY, 1992.
- G. Foley, A review of factors affecting filter cake properties in dead-end micro-
- filtration of microbial suspensions, J. Membr. Sci. 274 (2006) 38-46.
- R.W. Field, D. Wu, J.A. Howell, B.B. Gupta, Critical flux concept for microfiltration fouling, J. Membr. Sci. 100 (1995) 259-272. P. Bacchin, P. Aimar, R.W. Field, Critical and sustainable fluxes: theory, experi-
- ments and applications, J. Membr. Sci. 281 (2006) 42-69.
- [6] D. Elzo, I. Huisman, E. Middelink, V. Gekas, Charge effects on inorganic membrane performance in a cross-flow microfiltration process, Coll. Surf. A Physicochem. Eng. Asp. 138 (1998) 145–159.
- M.T. Aspelund, C.E. Glatz, Clarification of aqueous corn extracts by tangential flow microfiltration, J. Membr. Sci. 365 (2010) 123-129.
- [8] P.G. Middlewood, J.K. Carson, Extraction of amaranth starch from an aqueous medium using microfiltration: membrane characterisation, J. Membr. Sci. 405-406 (2012) 284–290.
- P.G. Middlewood, J.K. Carson, Extraction of amaranth starch from an aqueous medium using microfiltration; membrane fouling and cleaning, J. Membr, Sci. 411-412 (2012) 22-29.
- T. Maruyama, S. Katoh, M. Nakajima, H. Nabetani, T.P. Abbott, A. Shono, K. Satoh, FT-IR analysis of BSA fouled on ultrafiltration and microfiltration membranes, J. Membr. Sci. 192 (2001) 201-207.

- [11] S.M. Dutczak, C.R. Tanardi, K.K. Kopeć, M. Wessling, D. Stamatialis, "Chemistry in a spinneret" to fabricate hollow fibers for organic solvent filtration, Sep. Purif. Technol, 86 (2012) 183-189.
- [12] C. Ursino, S. Simone, L. Donato, S. Santoro, M.P. De Santo, E. Drioli, E. Di Nicolo, A. Figoli, ECTFE membranes produced by non-toxic diluents for organic solvent filtration separation, RSC Adv. 6 (2016) 81001-81012.
- [13] H. Karkhanechi, S. Rajabzadeh, E. Di Nicolò, H. Usuda, A.R. Shaikh, H. Matsuyama, Preparation and characterization of ECTFE hollow fiber membranes via thermally induced phase separation (TIPS), Polymer 97 (2016) 515–524.
 [14] N. Yao, J. Chau, E. Elele, B. Khusid, K.K. Sirkar, D.J. Dehn, Characterization of
- microporous ECTFE membrane after exposure to different liquid media and radiation, J. Membr. Sci. 532 (2017) 89–104.
- [15] C.W. Extrand, The use of fluoropolymers to protect semiconductor materials, J. Fluor. Chem. 122 (2003) 121-124.
- E. Drioli, S. Santoro, S. Simone, G. Barbieri, A. Brunetti, F. Macedonio, A. Figoli, ECTFE membrane preparation for recovery of humidified gas streams using membrane condenser, React. Funct. Polym. 79 (2014) 1-7.
- [17] N. Yao, B. Khusid, K.K. Sirkar, D.J. Dehn, Effects of Tri-n-octylamine with or without diluents on microporous ethylene chlorotrifluoroethylene membranes. Indus. Eng. Chem. Res. 56 (2017) 9698-9709.
- [18] S. Lee, K.S. Knaebel, Effects of mechanical and chemical properties on transport in fluoropolymers. I. transient sorption, J. Appl. Polym. Sci. 64 (1997) 455–476.
- [19] M.S. Hedenqvist, J.E. Ritums, M. Condé-Brana, G. Bergman, Structure and properties of poly(ethylene-co-chlorotrifluoroethylene) and polyvinylidene fluoride exposed to water, hydrochloric acid, hydrobromic acid and tetrachloroethylene, Polym. Eng. Sci. 44 (2004) 113–122.
- [20] J. Pan, C. Xiao, Q. Huang, H. Liu, J. Hu, ECTFE porous membranes with conveniently controlled microstructures for vacuum membrane distillation, J. Mater. Chem. A 3 (2015) 23549-23559.
- [21] J. Pan, C. Xiao, Q. Huang, C. Wang, H. Liu, Fabrication and properties of poly (ethylene chlorotrifluoroethylene) membranes via thermally induced phase separation (TIPS), RSC Adv. 5 (2015) 45249-45257.
- [22] S. Simone, A. Figoli, S. Santoro, F. Galiano, S.M. Alfadul, O.A. Al-Harbi, E. Drioli, Preparation and characterization of ECTFE solvent resistant membranes and their application in pervaporation of toluene/water mixtures, Sep. Pur. Technol. 90 (2012) 147-161.
- [23] B. Zhou, Q. Li, Y. Tang, Y. Lin, X. Wang, Preparation of ECTFE membranes with bicontinuous structure via TIPS method by a binary diluent, Desal. Water Treat. 57 (2016) 17646-17657.
- F. Falbo, S. Santoro, F. Galiano, S. Simone, M. Davoli, E. Drioli, A. Figoli, Organic/ organic mixture separation by using novel ECTFE polymeric pervaporation membranes, Polymer 98 (2016) 110–117.
- J. Pan, C. Xiao, Q. Huang, H. Liu, T. Zhang, ECTFE hybrid porous membrane with hierarchical micro/nano-structural surface for efficient oil/water separation, J. Membr. Sci. 524 (2017) 623-630.
- [26] K. Smolders, A.C.M. Franken, Terminology for membrane distillation, Desalination 72 (1989) 249-262.
- [27] N. Yao, J. Chau, E. Elele, B. Khusid, K.K. Sirkar, Characterization of microporous ECTFE membrane after exposure to different liquid mediums and radiation, ECI: Membrane Technology VII, Cork, Ireland, 2016.
- [28] J. Mulder, Basic Principles of Membrane Technology, Springer Science & Business Media, 2012.
- [29] K.K. Sirkar, Separation of Molecules, Macromolecules and Particles: Principles, Phenomena and Processes, Cambridge University Press, 2014.
- [30] A. Lim, R. Bai, Membrane fouling and cleaning in microfiltration of activated sludge wastewater, J. Membr. Sci. 216 (2003) 279-290.
- M.R. Wiesner, S. Veerapaneni, D. Brejchová, Improvements in membrane microfiltration using coagulation pretreatment, September 28-30, 1992, Nice, France, in: R. Klute, H. Hahn (Eds.), Chemical Water and Wastewater Treatment II: Proceedings of the 5th Gothenburg Symposium, Springer Berlin Heidelberg, Berlin, Heidelberg, 1992, pp. 281-296.
- [32] M. Cheryan, Ultrafiltration Handbook, Technomic Publishing Co. Inc., 1986.
- [33] Z. Tadmor, C.G. Gogos, Principles of Polymer Processing, John Wiley & Sons, 2013.
- [34] R.B. Bird, W.E. Stewart, E.N. Lightfoot, Transport Phenomena, John Wiley & Sons Inc, USA, 2002.
- [35] G. Bristow, W. Watson, Cohesive energy densities of polymers. Part 1. —Cohesive energy densities of rubbers by swelling measurements, Trans. Faraday Soc. 54 (1958) 1731-1741.
- [36] G. Bristow, W. Watson, Cohesive energy densities of polymers. Part 2. —Cohesive energy densities from viscosity measurements, Trans, Faraday Soc. 54 (1958)
- [37] C.M. Hansen, The universality of the solubility parameter, Industrial & Eng Chem. Prod. Res. Development 8 (1969) 2-11.
- [38] A.F. Barton, CRC Handbook of Solubility Parameters and other Cohesion Parameters, CRC Press, 1991.
- M.A. Kader, A.K. Bhowmick, Thermal ageing, degradation and swelling of acrylate rubber, fluororubber and their blends containing polyfunctional acrylates, Polym. Degrad. Stab. 79 (2003) 283-295.
- [40] S. Ebnesajjad, Fluoroplastics, Volume 2: Melt Processible Fluoropolymers-The Definitive User's Guide and Data Book, William Andrew, 2015.
- J. Brandrup, E.H. Immergut, E.A. Grulke, A. Abe, D.R. Bloch, Polymer Handbook, John Wiley & Sons, New York, NY, 1989.
- [42] D.R. Machado, D. Hasson, R. Semiat, Effect of solvent properties on permeate flow through nanofiltration membranes. Part I: investigation of parameters affecting solvent flux, J. Membr. Sci. 163 (1999) 93-102.
- [43] G. Vazquez, E. Alvarez, J.M. Navaza, Surface tension of alcohol water + water from 20 to 50.degree. C, J Chem. Eng. Data 40 (1995) 611-614.
- [44] R.C. Weast, M.J. Astle, Handbook of Chemistry and Physics, 59th ed., CRC Press, Inc., West Palm Beach, FL, U.S.A., 1975.